Evolution of GaAs nanowire geometry in selective area epitaxy

Kevin P. Bassett, Parsian K. Mohseni, and Xiuling Li

Citation: Applied Physics Letters **106**, 133102 (2015); doi: 10.1063/1.4916347
View online: http://dx.doi.org/10.1063/1.4916347
View Table of Contents: http://scitation.aip.org/content/aip/journal/apl/106/13?ver=pdfcov
Published by the AIP Publishing

Evolution of GaAs nanowire geometry in selective area epitaxy

Kevin P. Bassett, Parsian K. Mohseni, and Xiuling Li[a)]
Department of Electrical and Computer Engineering, Micro and Nanotechnology Laboratory, International Institute for Carbon-Neutral Energy Research (I²CNER), University of Illinois at Urbana-Champaign, Urbana, Illinois 61801, USA

(Received 30 January 2015; accepted 16 March 2015; published online 31 March 2015)

Nanowires (NWs) grown via selective area epitaxy (SAE) show great promise for applications in next generation electronic and photonic devices, yet the design of NW-based devices can be complicated due to the complex kinetics involved in the growth process. The presence of the patterned selective area mask, as well as the changing geometry of the NWs themselves during growth, leads to non-linear growth rates which can vary significantly based on location in the mask and the NW size. Here, we present a systematic study of the evolution of GaAs NW geometry during growth as a function of NW size and pitch. We highlight a breakdown of NW uniformity at extended growth times, which is accelerated for NW arrays with larger separations. This work is intended to outline potential fundamental growth challenges in achieving desired III–V NW array patterns and uniformity via SAE. © *2015 AIP Publishing LLC*. [http://dx.doi.org/10.1063/1.4916347]

Semiconductor nanowires (NWs) grown by the selective area epitaxy (SAE) technique have recently been shown to be promising for various photonic and electronic device applications.[1] Many SAE-NW-based devices have recently been demonstrated including photonic crystal cavities,[2] Fabry-Perot resonators,[3] lasers,[4] photo-detectors,[5,6] and various solar cell designs.[7–9] In addition, research demonstrating the direct growth of compound semiconductor SAE-NWs on silicon has shown a pathway to direct integration of photonic devices onto CMOS chips, possibly providing a much sought after solution to a long standing technical challenge.[10,11] A major advantage of the SAE technique over other growth methods is the inherent lithographic control of the location and size of the wires; making it possible to design site-controlled, array-based devices. Furthermore, the SAE approach circumvents notable challenges associated with Au-mediated vapor-liquid-solid (VLS) NW growth, such as morphological non-homogeneity,[12] phase-segregation in ternary/quaternary alloys,[13] and Au precipitant contamination.[14]

Many NW-based device demonstrations have involved NWs randomly located on a sample due to the nature of the self-assembly process.[15–17] This presents a challenge for integration and makes precisely ordered arrays, necessary for some device designs, impossible. The SAE-NW technique can solve this issue by using a lithographically defined growth mask to precisely locate and control the size of the wires. However, the presence of the growth mask required in the SAE approach causes an enhancement of epitaxial growth in the local area around the growth mask due to surface diffusion, a well-known phenomenon in thin film SAE.[18,19] Since the presence of the mask modulates the local partial pressure of precursors in a given growth area on the substrate, local enhancement can vary between different growth species due to their different diffusion properties, thus, resulting in locally varying ternary and quaternary compositions.[20] In addition to these common SAE effects, the SAE-NW technique suffers from additional complications due to the increased surface-area-to-volume ratio and introduction of large sidewall facets during growth. The geometry of the NW array itself can also cause a relative enhancement in a local area due to dynamic vapor phase diffusion and adsorption processes. Both of these departures from conventional thin film SAE will be discussed in relation to experimental results in this work. Additionally, the SAE-NW growth process may not be completely selective along the NW axial direction and the existence, although small, of a competing growth mode on the {110} sidewalls of the NWs cannot be completely ignored in order to precisely predict the final dimensions of a NW-based periodic array, and is even further complicated in the case of aperiodic arrays (i.e., photonic crystal waveguides and defect cavities). The combination of these factors motivates an in-depth study to further the understanding of the complex growth process. In this work, we present a systematic study of SAE-based GaAs NW growth and quantify the effect of the selective area mask pore size (D_P) and pitch (a) on the evolution of the wires.

We have observed that while radial growth of NWs remains roughly constant and linear with time, axial growth exhibits a trend in which a slower initial growth regime precedes a linear, steady-state growth regime, in which the growth rate trails off. Since pattern geometry and resulting NW morphology vary significantly for the structures studied, we also present volumetric analysis of the growth data. Through volumetric analysis, it can be seen that the rate of material volume addition is nearly constant over the changing pattern geometry, with a slight variation in volume addition rate with time, explained by variable onset of the saturation region based on pattern geometry. Hexagonal geometry is shown to break down, likely due to synergetic growth effects[21] once a threshold is reached, eventually turning a NW array into a coalesced block. This threshold depends on the enhancement ratio of a given pattern and the spacing between NWs. This work highlights the growth window conducive to the synthesis of NW arrays with perfectly

[a)]Author to whom correspondences should be addressed. Electronic mail: xiuling@illinois.edu

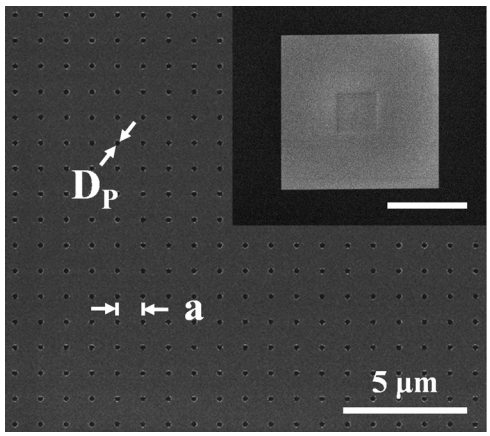

FIG. 1. Plan-view SEM image of pattern area showing the square lattice of pores. Pore diameter and pitch are labelled as D_P and a, respectively. Inset shows a SEM image of a 100 μm × 100 μm electron-beam lithography patterned array of pores in a 400 μm × 400 μm SiO_2 mesa (inset scale bar represents 200 μm).

hexagonal geometries and shows the challenges associated with SAE beyond these boundaries.

Selective-area epitaxial growth masks were made by depositing 20 nm SiO_2 onto GaAs substrates via plasma-enhanced chemical vapor deposition (PECVD), followed by lithography to define the growth mask, which was carried out on a Raith e-line electron-beam lithography system. Growth templates consisted of 100 μm × 100 μm arrays of pores with an oxide skirt size (mesa) of 400 μm × 400 μm. Arrays varied in pore diameter from 125 nm to 225 nm (50 nm incremental) and in pitch from 1 μm to 0.6 μm (100 nm incremental). The constant array-to-oxide skirt size was chosen to eliminate enhancement effects for all samples studied. An example of the mask pattern prior to growth is shown in Figure 1.

Growth was carried out in an AIXTRON AIX-200/4 MOCVD system. Trimethyl-gallium (TMGa) and arsine (AsH_3) were used as group-III and group-V precursors, respectively. Nanowire growth was performed at 750 °C at 50 mbar total pressure with palladium-diffused hydrogen (H_2) as the carrier gas. A native oxide desorption step was carried out at 800 °C under a constant AsH_3 flow. The total growth time was 80 min, broken into four consecutive 20 min growths, after each of which, observations were made via scanning electron microscopy (SEM) using a Hitachi S-4800. It should be noted that the above growth conditions are representative of a comparable parameter space as previous reports on SAE-grown GaAs NWs, as presented in Table I.

Unity NW growth yields are achieved (i.e., every pore leads to a vertical GaAs NW) over all the arrays investigated, as shown in the supplementary material.[28] Examples of the resulting NWs grown by the SAE method are shown in Figure 2. All frames of Figure 2 were taken after growth step 2 (t = 40 min). The top pair of rows shows plan-view and 30° tilted-view SEM images of the largest array pitch (1 μm), while the bottom pair of rows shows the same for the smallest array pitch (600 nm). As expected and seen in the tilted-view panels in Figure 2, an inverse proportionality exists between NW length and pore diameter. This will be explored in detail with regard to volumetric growth conservation below. We further note that epitaxial registry exists between the substrate and the NWs (vertical NW growth is found on a (111)B surface) and that hexagonal NW symmetry is preserved with parallel {110} oriented sidewall facets observed amongst neighboring NWs.

The evolution of NW geometry with time is shown in Figure 3. Thirty degree tilted-view SEM images of the same pattern across the four growth steps are shown. To eliminate sample to sample patterning variation and for self-consistency, the initial growth was followed by three re-growth steps on the same template. In addition to the desired axial growth of the NWs in time, the smaller, yet non-trivial, radial growth can also be clearly observed as evidenced by the reduced gap between nearest neighbor NWs. This trend will be quantified later in the discussion of detailed measurements presented in Figure 4. To quantify crystal growth evolution trends, NW lengths and diameters were measured via SEM after each of the four growth steps. Every data point represents an average value taken from at least 10 individual NWs, with error bars showing the approximate maximum and minimum deviation range from the mean. Large area analysis demonstrated consistent growth trends as compared to the smaller sample sets measured. An image processing program[29] was used to measure and average the area of the

TABLE I. Comparison of the growth conditions for this study to other published work on SAE-grown GaAs NWs. Note for core-shell or QW/QD structures only the base GaAs NW is considered.

	Growth Temperature (°C)	Pressure (atm)	TMGa partial pressure (atm)	AsH3 partial pressure (atm)	V/III ratio
This work	750	0.097	2.7×10^{-6}	2.5×10^{-4}	93
Hokkaido[22]	750	0.1	2.7×10^{-6}	2.5×10^{-4}	93
Hokkaido[23]	750	0.1	2.7×10^{-7}	2.5×10^{-4} to 1.7×10^{-3}	926–6296
Hokkaido[24]	700–850	0.1	2.7×10^{-6}	2.5×10^{-5} to 5.0×10^{-4}	9.3–185
Hokkaido[25]	750	0.1	2.7×10^{-6}	5.0×10^{-4}	185
Hokkaido[10]	750	0.1	8.2×10^{-7}	2.5×10^{-4}	305
UCLA[2,4]	735	0.079	…[a]	…[a]	…[a]
UCLA[6,26]	720	0.079	…[a]	…[a]	9
USC[9,27]	700	0.1	3.8×10^{-7}	7.1×10^{-5} to 2.4×10^{-4}	189–643
USC[3,5]	760	0.1	7.6×10^{-7}	2.1×10^{-4}	283
USC[1]	790	0.1	3.7×10^{-7}	4.8×10^{-5}	127

[a]Undisclosed information.

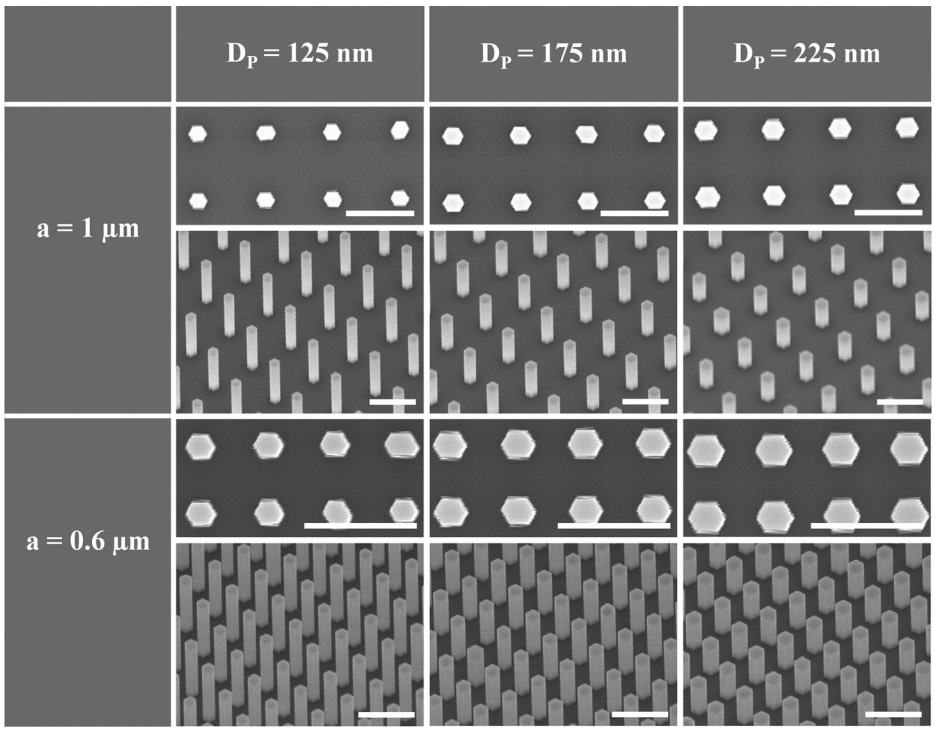

FIG. 2. Plan-view and 30° tilted-view SEM images of SAE-grown GaAs NWs. Patterned pore diameter varies across columns: 125 nm, 175 nm, and 225 nm. The second and fourth rows are tilted views of the first and third rows. D_P and a define the lithographically patterned pore diameter and pitch, respectively. Pitch varied from 1 μm in the first row to 600 nm in the third row. Note that the magnification varies in all rows. However, all scale bars are 1 μm.

end facets of the NWs. Diameter was defined as the length across a perfect hexagon from point to point with equivalent area, by use of the following equation:

$$D_{PerfectHexagon} = 2 * \sqrt{\frac{2}{3 * \sqrt{3}} * A_{Measured}}. \quad (1)$$

The use of this calculation allowed us to meaningfully assess the addition of material volume across growth steps as perfect hexagonal symmetry began to break down. Simply measuring the Feret diameter of the NWs as they evolve and become less symmetric would not yield an accurate NW volume once those Feret diameters were used to calculate hexagonal area and multiplied by length. The resulting measurements of length and diameter are plotted in Figure 4.

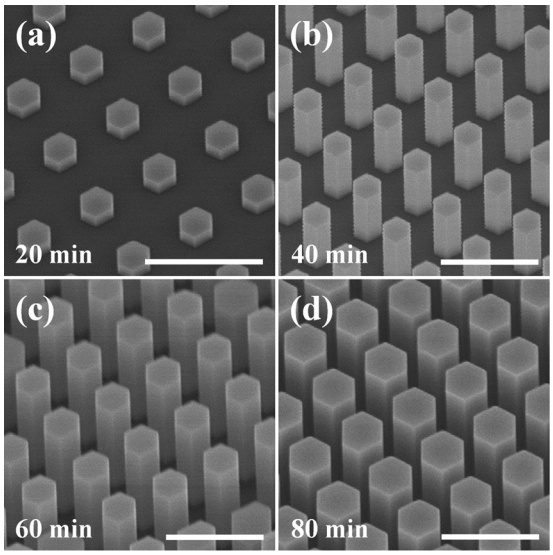

FIG. 3. 30° tilted SEM images of the time evolution of NW geometry over the four growth steps (t = (a) 20, (b) 40, (c) 60, and (d) 80 min) for a 600 nm pitch and 225 nm diameter pore array. All scale bars represent 1 μm.

In the final region, saturation of the axial growth rate begins. While the slow growth rate experienced in the first growth regime could be explained as a growth nucleation effect, this nucleation phase also exists before each growth step, as the same sample was re-grown for each data set. Instead, the growth is actually limited by the initially small surface area of the pores that are unable to capture all available growth species before they diffuse to adjacent unpatterned growth areas, which act as a large material sink. Once the NWs reach some initial length, they have sufficient surface area to fully capture all the limiting material precursors before they diffuse away. Once this minimum surface area is reached, the maximum axial growth rate is reached in turn, and the main linear growth regime begins. This linear growth continues until the radial expansion of the wires reaches a point at which gaps between the wires start to limit diffusion in the gas phase to the sidewalls. At this point, the effective surface area of the NWs in the array for adsorbing precursors from the gas phase starts to decrease, leading to lower effective growth rates. Although the above length and diameter evolution trends, shown in Figure 4(a), are useful for targeting specific NW geometries, they show an incomplete view of the overall selective area growth kinetics. For a more complete picture, we are interested in understanding the evolution of NW volumes during SAE. In Figures 4(b) and 4(c), the average NW volume vs. time and corresponding volumetric growth rate vs. time are plotted, respectively. In Figure 4(b), we note an exponentially increasing trend at each time interval, indicating an accelerating volumetric growth rate. This is a significant observation, which differs dramatically from the linear growth trend of conventional two-dimensional (2D) film SAE. The prominent difference between 2D SAE and NW-SAE is the constant geometry of

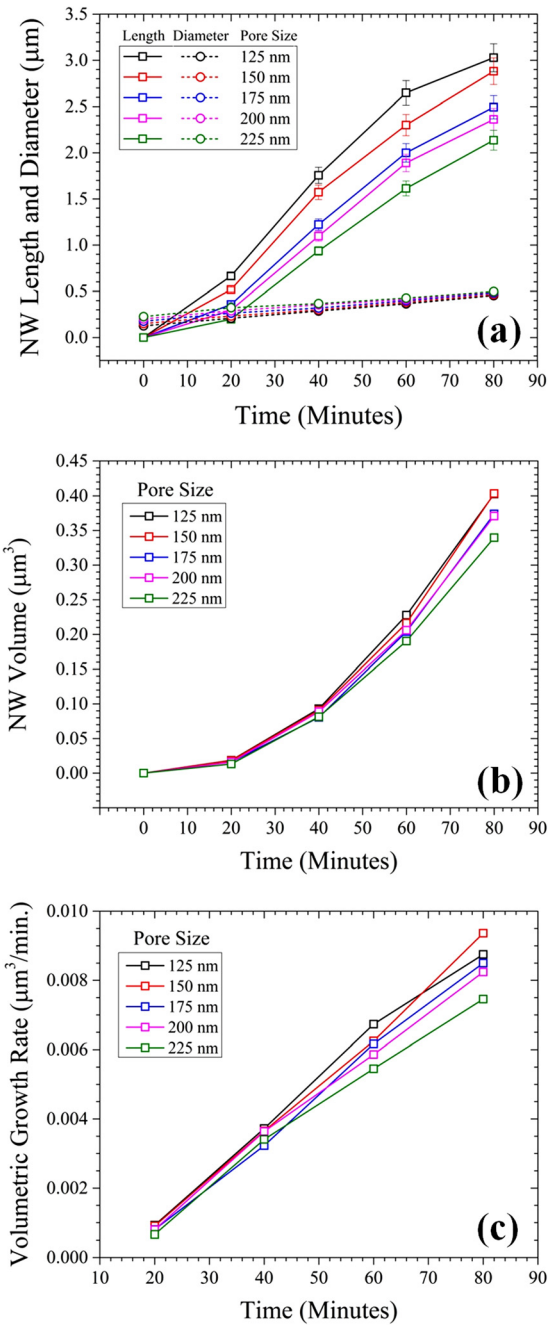

FIG. 4. (a) Plot of NW length and diameter vs. growth time for patterns with a 600 nm pitch. Error bars represent the maximum and minimum deviation from the mean (smaller deviation values are hidden data points). The radial growth rate is significantly smaller than the axial growth rate as expected for SAE NW growth. However, note that the radial growth rate is not zero (4.1 and 2.9 nm/min for 125 and 225 nm pores, respectively) and is approximately linear, in contrast to the non-linear axial growth. (b) Plot of NW volume vs. growth time for patterns with a 600 nm pitch as calculated from measurements of length and cross-sectional area via SEM. (c) Plot of NW volumetric growth rate derived from the data of (b). Note the linearity of the plot indicating constant volume addition to the NW with time.

the former and the variable geometry of the latter, which introduces new surfaces for material capture as growth continues. Whereas for planar SAE structures, a constant exposed area exists for nucleation of vapor-phase growth species, the material sink for NW geometries is continually increasing through the introduction of actively expanding surfaces that can capture diffusive adatoms. Within the parameter space explored in the current study, NW growth evolution is neither simply limited by surface diffusion of growth species nor by the supply of adatoms from the surrounding vapor phase. Rather, the most influential factor that determines NW volumetric growth is the geometry of the individual NWs comprising the array. Based on the previous NW-SAE reports for InAs,[30] we should expect to exit the geometry-limited regime and enter a surface diffusion-limited regime in which volumetric growth rate becomes constant at extended growth times. However, as supported by Figure 4(c), our volumetric growth rate is monotonically increasing for all time intervals and pore sizes. The current increasing growth rate trend can be justified by considering the diffusion length discrepancy between In and Ga, since the onset of a diffusion-limited growth regime, relative to one that is geometry-limited, is expedited for shorter diffusion lengths.

Under the conditions explored here, an even more dramatic evolution in NW growth is observed prior to the onset of diffusion-limited volumetric growth rate saturation; namely, the breakdown of NW hexagonal symmetry. As growth evolves, the hexagonal symmetry of the NWs begin to degrade in patterns where the gaps between NWs have decreased due to the radial growth. Such a geometric breakdown effect is quantified in Figure 5, where hexagonally symmetric NW yield (fraction of NW grown with equilateral hexagonal cross-sections) is plotted as a function of growth time. We note that as the growth time increases, the yield of hexagonally symmetric NWs decreases such that, in the most extreme scenario, only ~60% of all NWs in an array have preserved their original geometries. The tilted-view SEM images shown as insets in Figure 5 demonstrate the noted breakdown phenomenon, which can likely be attributed to synergetic growth effects[21] arising from substantial radial growth (reduced nearest neighboring NW distance) at extended growth times. This can become a runaway effect, eventually filling the entire array in and forming a large coalesced block. Further validation of the synergetic growth phenomenon is presented in the supplementary material.[28]

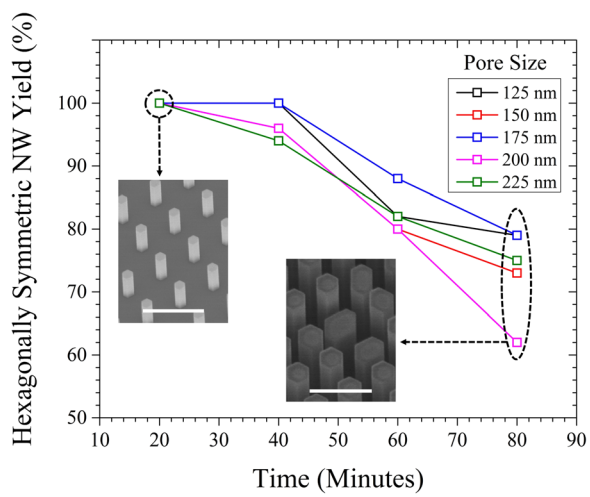

FIG. 5. Measured yield of hexagonally symmetric NWs as a function of growth time. Insets show representative tilted-view SEM images of as-grown NW arrays with identical pore diameter ($D_P = 125$ nm) and pitch values ($a = 600$ nm) after 20 min (left) and 80 min (right) of growth. Inset scale bars represent 1 μm.

Asymmetric NW growth at extended periods was not observed to vary along the length of the NWs. As such, symmetry breakdown did not result in the formation of NWs with tapered geometries. Finally, it should be noted that since SAE NW growth evolution depends strongly on the pitch of pore patterns, such that growth rate trends are exaggerated for larger pitch values, breakdown of hexagonal symmetry was observed at shorter growth times for pitch values greater than 600 nm. As such, our systematic study of growth trends was limited to patterns with $P = 600$ nm.

High-resolution transmission electron microscopy analysis reveals that NWs grown under these conditions exhibit a polytypic crystal structure composed of a predominant zinc-blende lattice with high density incorporation of lateral stacking faults. Room-temperature photoluminescence (PL) spectra taken from these NW arrays show strong emission centered at ~870 nm along with resonant cavity mode-like peaks, implying good optical quality of the NWs. Further analysis of both the TEM and PL results will be reported separately.

In summary, we have presented an in-depth study of GaAs NW growth evolution via SAE. Examinations of growth rate trends based on systematic growth studies allowed for an understanding of the complex growth kinetics present during III–V NW-SAE and provided insights into the capabilities and limitations inherent to the technique. An analysis of NW growth rate based on volume allowed us to establish the prevalence of a geometry-limited growth regime prior to the onset of diffusion-limited growth. Furthermore, a breakdown of hexagonal symmetry in NW cross-section was observed for a combination of sufficiently high growth enhancement and narrow gap between adjacent wires. Knowledge of the ideal growth boundaries, which define the limits before the onset of growth homogeneity breakdown, will aid in future device designs where a perfect hexagonal NW morphology is highly desirable. These guidelines for symmetrically hexagonal NW growth and defective growth mitigation techniques may be adopted based on these findings to either discourage or encourage the formation of coalesced structures as the device designer intends. The trends presented herein should provide direction for device designers targeting specific SAE-NW geometries for applications in a myriad of active and passive device designs.

This work was supported in part by the U.S. Department of Energy, Office of Science, Basic Energy Sciences, under award DE-FG02-07ER46741.

[1]S. Hu, C.-Y. Chi, K. T. Fountaine, M. Yao, H. A. Atwater, P. D. Dapkus, N. S. Lewis, and C. Zhou, Energy Environ. Sci. **6**, 1879 (2013).
[2]A. C. Scofield, J. N. Shapiro, A. Lin, A. D. Williams, P.-S. Wong, B. L. Liang, and D. L. Huffaker, Nano Lett. **11**, 2242 (2011).
[3]S. Arab, P. D. Anderson, M. Yao, C. Zhou, P. D. Dapkus, M. L. Povinelli, and S. B. Cronin, Nano Res. **7**, 1146 (2014).
[4]A. C. Scofield, S.-H. Kim, J. N. Shapiro, A. Lin, B. Liang, A. Scherer, and D. L. Huffaker, Nano Lett. **11**, 5387 (2011).
[5]M. A. Seyedi, M. Yao, J. O'Brien, S. Y. Wang, and P. D. Dapkus, Appl. Phys. Lett. **103**, 251109 (2013).
[6]P. Senanayake, A. Lin, G. Mariani, J. Shapiro, C. Tu, A. C. Scofield, P.-S. Wong, B. Liang, and D. L. Huffaker, Appl. Phys. Lett. **97**, 203108 (2010).
[7]G. Mariani, R. B. Laghumavarapu, B. Tremolet de Villers, J. Shapiro, P. Senanayake, A. Lin, B. J. Schwartz, and D. L. Huffaker, Appl. Phys. Lett. **97**, 013107 (2010).
[8]G. Mariani, P.-S. Wong, A. M. Katzenmeyer, F. Léonard, J. Shapiro, and D. L. Huffaker, Nano Lett. **11**, 2490 (2011).
[9]M. Yao, N. Huang, S. Cong, C.-Y. Chi, M. A. Seyedi, Y.-T. Lin, Y. Cao, M. L. Povinelli, P. D. Dapkus, and C. Zhou, Nano Lett. **14**, 3293 (2014).
[10]K. Tomioka, J. Motohisa, S. Hara, K. Hiruma, and T. Fukui, Nano Lett. **10**, 1639 (2010).
[11]Z. Zhao, K. Yadavalli, Z. Hao, and K. L. Wang, Nanotechnology **20**, 035304 (2009).
[12]M. C. Plante and R. R. Lapierre, Nanotechnology **19**, 495603 (2008).
[13]Y.-N. Guo, H.-Y. Xu, G. J. Auchterlonie, T. Burgess, H. J. Joyce, Q. Gao, H. H. Tan, C. Jagadish, H.-B. Shu, X.-S. Chen, W. Lu, Y. Kim, and J. Zou, Nano Lett. **13**, 643 (2013).
[14]J. E. Allen, E. R. Hemesath, D. E. Perea, J. L. Lensch-Falk, Z. Y. Li, F. Yin, M. H. Gass, P. Wang, A. L. Bleloch, R. E. Palmer, and L. J. Lauhon, Nat. Nanotechnol. **3**, 168 (2008).
[15]P. K. Mohseni, A. Behnam, J. D. Wood, X. Zhao, K. J. Yu, N. C. Wang, A. Rockett, J. A. Rogers, J. W. Lyding, E. Pop, and X. Li, Adv. Mater. **26**, 3755 (2014).
[16]J. C. Shin, P. K. Mohseni, K. J. Yu, S. Tomasulo, K. H. Montgomery, M. L. Lee, J. A. Rogers, and X. Li, ACS Nano **6**, 11074 (2012).
[17]J. C. Shin, A. Lee, P. K. Mohseni, D. Y. Kim, L. Yu, J. H. Kim, H. J. Kim, W. J. Choi, D. Wasserman, K. J. Choi, and X. Li, ACS Nano **7**, 5463 (2013).
[18]J. J. Coleman, Proc. IEEE **85**, 1715 (1997).
[19]V. C. Elarde, T. S. Yeoh, R. Rangarajan, and J. J. Coleman, J. Cryst. Growth **272**, 148 (2004).
[20]M. Alam, R. People, and E. Isaacs, Appl. Phys. Lett. **74**, 2617 (1999).
[21]M. T. Borgström, G. Immink, B. Ketelaars, R. Algra, and E. P. A. M. Bakkers, Nat. Nanotechnol. **2**, 541 (2007).
[22]J. Motohisa, J. Noborisaka, J. Takeda, M. Inari, and T. Fukui, J. Cryst. Growth **272**, 180 (2004).
[23]J. Noborisaka, J. Motohisa, and T. Fukui, Appl. Phys. Lett. **86**, 213102 (2005).
[24]J. Motohisa, Physica E **23**, 298 (2004).
[25]A. Hayashida, T. Sato, S. Hara, J. Motohisa, K. Hiruma, and T. Fukui, J. Cryst. Growth **312**, 3592 (2010).
[26]J. N. Shapiro, A. Lin, P. S. Wong, A. C. Scofield, C. Tu, P. N. Senanayake, G. Mariani, B. L. Liang, and D. L. Huffaker, Appl. Phys. Lett. **97**, 243102 (2010).
[27]A. R. Madaria, M. Yao, C. Chi, N. Huang, C. Lin, R. Li, M. L. Povinelli, P. D. Dapkus, and C. Zhou, Nano Lett. **12**, 2839 (2012).
[28]See supplementary material at http://dx.doi.org/10.1063/1.4916347 for demonstration of the uniformity over a large area of the nanowire arrays in this work as well as support for synergetic growth effects.
[29]C. A. Schneider, W. S. Rasband, and K. W. Eliceiri, Nat. Methods **9**, 671 (2012).
[30]S. Hertenberger, D. Rudolph, M. Bichler, J. J. Finley, G. Abstreiter, and G. Koblmuüller, J. Appl. Phys. **108**, 114316 (2010).